

Vibrational properties of epitaxial graphene buffer layer on silicon carbide

Guillaume Radtke^{1,*} and Michele Lazzeri¹

¹*Sorbonne Université, CNRS UMR 7590, MNHN, IMPMC, 4 place Jussieu, 75252 Paris, France*

The vibrational properties of semiconducting graphene buffer layer epitaxially grown on hexagonal silicon carbide are determined using first-principles calculations on a realistic structural model. Despite the important chemical and structural disorder associated with the partial covalent bonding with the substrate, the buffer-layer carbon atoms still display quasi-dispersive phonons mimicking those of graphene. The related frequency softening and broadening provide a natural interpretation of the measured Raman signal. The vibrations determining thermal conduction are found to delocalize completely on the SiC substrate, leading to an effective spatial separation between material components determining, respectively, electronic and thermal transport properties. This situation opens perspectives for thermoelectric applications.

The term *buffer layer* (BL) commonly refers to the first graphitic layer formed after high-temperature silicon sublimation from a silicon carbide (SiC) substrate. The BL has been known for decades but mainly considered as an unwanted byproduct of the epitaxial growth of 'proper' graphene, which forms subsequently. The BL in itself started attracting a specific interest only in recent years [1–4]. Indeed, although this atomic layer retains the overall two-dimensional honeycomb structure of graphene, the partial covalent interaction with the substrate leads to a drastic modification of its electronic structure. In particular, the observation of a band gap of the order of 0.5 eV can be a substantial advantage over semi-metallic graphene [3]. Besides, very recently, room temperature hole mobilities exceeding $5000 \text{ cm}^2 \text{ V}^{-1} \text{ s}^{-1}$ were measured on macroscopic domains of SiC covered with this long-range ordered semiconducting carbon layer [4], renewing the interest in the BL as a potential candidate for beyond-silicon electronics [5].

There is an overall consensus on the BL atomic structure, deduced from low-energy electron diffraction [4, 6–9] and described as a 13×13 graphene supercell covalently bonded to an underlying Si-terminated SiC (0001) surface. In this large cell, known as the $(6\sqrt{3} \times 6\sqrt{3})R30^\circ$ reconstruction and thoroughly investigated numerically [10–13], only a fraction of the BL carbon atoms are bonded to the underlying Si atoms. This results in a complex structure where each carbon is surrounded by a different environment, providing a locally disordered form of graphene.

Whereas vibrational properties of single and many-layer graphene have been extensively investigated and are now well understood [14–16], little is known on those of the BL, in spite of their fundamental character. Besides, phonons are the main heat carriers in semiconductors and play a central role in various applications. In this context, we stress that the poor thermoelectric properties of graphene are largely due to a small Seebeck coefficient, related to its gapless electronic structure, but also to a very high thermal conductivity [17]. An important effort

has therefore been devoted to improve its thermoelectric figure of merit, through defect engineering or composite design [18, 19]. Compared to graphene, the epitaxial BL on SiC displays the advantage of combining a sizeable electronic band gap, a high charge carrier mobility and, possibly, a smaller thermal conductivity due to the different atomic structure.

The little information available on BL vibrational properties can be attributed, experimentally, to the difficulty to grow large and homogeneous areas of high-quality material and, theoretically, to the large size of a realistic structure. Indeed, the reported Raman spectra acquired on BLs display significant differences [20], possibly due to samples inhomogeneity, and the few theoretical works specifically devoted to the investigation of vibrations used a small, unrealistic, $(\sqrt{3} \times \sqrt{3})R30^\circ$ reconstruction to approximate the structure [21–23].

In fact, the study of vibrations in the BL/SiC system requires the implementation of specific techniques beyond the standard ones used for *ab initio* lattice dynamics [24, 25]. As a consequence, a series of relevant questions remain open. For instance, considering this system as a prototypical form of disordered graphene, to which extent do the BL vibrational properties resemble those of pristine graphene? What is the origin of the specific Raman signatures visible on the BL spectra? More important, what is the thermal conductivity of the BL and how does it couple (thermal conductance) with the SiC substrate? Surprisingly, at present, it is not even clear whether these quantities are meaningful, given the strong covalent interaction occurring between the BL and the substrate.

In this Letter, we address these questions by determining fully *ab initio* the vibrational properties of the BL/SiC system within a realistic structural model. Calculations were performed using density functional theory [24–27]. Due to the very large system size, a strategy similar to the one developed in Refs. [28–30] is mandatory: the interatomic force constants (IFCs) were first calculated *ab initio* on a structure describing the interface and subsequently combined with those obtained from an independent calculation of bulk 4H-SiC, to construct the dynamical matrix of a slab containing L_{SiC} number of

* Corresponding author: guillaume.radtke@sorbonne-universite.fr

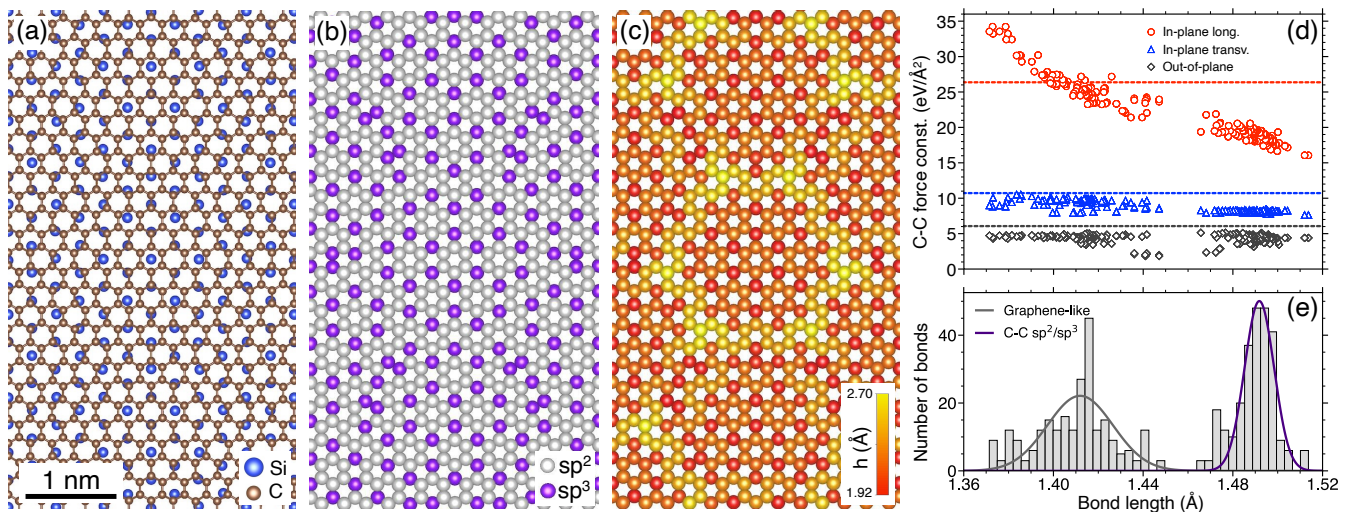


FIG. 1. (a) Top view of the relaxed atomic structure of the $(6\sqrt{3} \times 6\sqrt{3})R30^\circ$ surface reconstruction. Only the carbon atoms of the BL and the topmost Si layer of the substrate is shown. (b) Distribution of the sp^2 and sp^3 hybridized carbon atoms in the BL. (c) Height map of the BL carbon atoms. The zero is the average height of the topmost Si layer of the substrate. (d) IFCs between nearest neighbors atoms within the BL calculated for displacements perpendicular (out-of-plane) or within the atomic plane (in-plane, longitudinal or transverse to the bond direction). Horizontal lines are the respective quantities calculated for graphene. The IFCs are reported as a function of the bond length. (e) Histogram distribution of the C-C bond length. The two Gaussian distributions correspond to graphene-like and single C-C sp^2/sp^3 group of bonds.

SiC layers. The BL/SiC interface was modeled with the $(6\sqrt{3} \times 6\sqrt{3})R30^\circ$ reconstruction (*i.e.* 338 carbon atoms, only in the BL). The vibrational properties of the semi-infinite substrate were then obtained by adding successive SiC layers until convergence. While most of the properties are converged for $L_{\text{SiC}} = 10$ (~ 2500 atoms in total), calculations up to $L_{\text{SiC}} = 30$ (~ 6800 atoms) were necessary. Extrapolation for $L_{\text{SiC}} \rightarrow \infty$ is reported for specific properties. Further details are given as Supplemental Material (SM) [31].

A top view of the BL atomic structure is shown in Figure 1(a). A strong covalent interaction occurs between the BL carbon atoms and the topmost unsaturated silicon atoms which fall in close coincidence. Based on both the presence of a short Si-C bond length (~ 2 Å) and a substantial charge density localized between the atoms, about 26 % of the BL carbon atoms are found to adopt an sp^3 -like hybridization while the remaining atoms keep their sp^2 configuration, in good agreement with XPS results [2]. A representation of the spatial distribution of the sp^2/sp^3 atoms is shown in Figure 1(b). The consequences of the electron density redistribution within the BL clearly appear in the C-C bond length distribution. Indeed, Figure 1(e) shows two well-separated groups of bonds centered on 1.41 Å, close to the equilibrium C-C distance in graphene, and on 1.49 Å, representative of typical C-C sp^2/sp^3 single bonds [32]. Another consequence is the large deviation of the carbon layer from the ideal flat structure resulting in a significant rippling of the surface, see Figure 1(c). The alternation of crests and lower terraces of about 2 nm size approximately reproduces the (6×6) periodicity observed in STM measure-

ments [3, 33] and previous *ab initio* calculations [10–13]. While these terraces are tightly bound to the substrate through a high density of intruding carbon atoms [in red in Figure 1(c)], the crests are essentially involving sp^2 carbons which do not interact covalently with the substrate. The resulting average BL/substrate distance is 2.3 ± 0.2 Å in agreement with transmission electron microscopy [34] and X-ray reflectivity measurements [35].

The BL structure is therefore that of an overall two-dimensional hexagonal lattice of carbon atoms affected by a strong local structural and chemical disorder. This is reflected in the IFCs, which determine vibrational frequencies. For instance, the IFCs between nearest neighbors in the BL reported in Figure 1(d) are significantly scattered (see also SM [31]). This is accompanied by a global softening *w.r.t.* to graphene IFCs of 10 % for the in-plane longitudinal and up to 30 % for the out-of-plane components, on average. Note that the observed behavior is not trivial. For example, for the out-of-plane IFCs, it is reasonable to expect that the strong Si-C covalent interaction would lead to an IFCs softening. It is however counter-intuitive that this softening is affecting *all* C-C pairs, not only those located on the specific sites involving a Si-C bond.

We now discuss the projected phonon density of states (PPDOS) associated to different layers of the BL/SiC interface, since these quantities are nowadays measurable by electron energy loss spectroscopy [28]. Given a vibrational normal mode $|e_\nu\rangle$ with frequency ω_ν , $\langle l, r | e_\nu \rangle$ indicates its component on atom r of layer l . The PPDOS

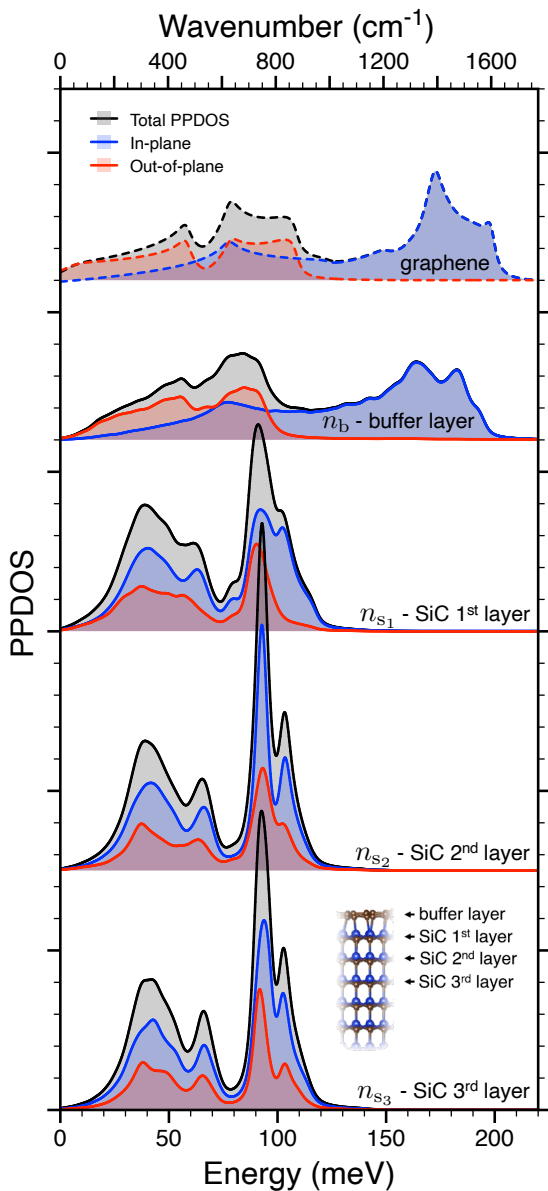


FIG. 2. Projected phonon densities of states (PPDOS) on the buffer layer (n_b) and on the top three SiC layers of the substrate (n_{s_1} , n_{s_2} , n_{s_3}) for the BL/SiC interface. As a comparison, the phonon density of states for pristine graphene is shown in the topmost panel.

on a layer l is defined as

$$n_l(\omega) = \frac{1}{N_l N_{\mathbf{q}}} \sum_{\nu, r} |\langle l, r | e_{\nu} \rangle|^2 \delta(\omega - \omega_{\nu}), \quad (1)$$

where the first sum runs over all the modes ν chosen on a grid of $N_{\mathbf{q}}$ wavevectors of the supercell Brillouin zone and the second one over the N_l atoms of the layer (the compound index r also includes the three Cartesian components) [31]. According to Figure 2, starting from the second layer, the PPDOS of the SiC is not substantially different from that of bulk hexagonal SiC, shown in SM [31].

The minor differences between the 2nd and the 3rd SiC layers are due to their inequivalence in the 4H stacking of bulk SiC. Finally, a pronounced disorder-induced broadening is observed for the topmost SiC layer. More significant modifications appear when comparing the PPDOS of the BL with the PDOS of perfect graphene, also reported in Figure 2. Although their overall shape remains similar, a sizeable broadening and global redshift is observed. This is particularly visible in the 150-200 meV (~ 1200 -1600 cm^{-1}) range of optical phonons where a downshift of about 10 meV ($\sim 80 \text{ cm}^{-1}$) of the leading peaks is observed.

To gain further insight into these results, we remark that the BL vibrations can be considered as those of a disordered 13×13 graphene supercell and, thus, unfolded onto the phonons of the 1×1 graphene unit cell. (More precisely, since the vibrational modes are defined on the whole BL/SiC slab, we are considering their component on the atoms of the BL.) Graphene phonons are defined on wavevectors \mathbf{q} of the graphene Brillouin zone and the unfolding produces a spectral function $S_b(\omega, \mathbf{q})$ (see SM [31] for the mathematical definition). S_b reveals to which extent the supercell modes inherit the translational symmetry of the 1×1 crystal: if S_b is calculated for a supercell of perfect graphene, it will provide its phonon dispersion whereas the presence of localized vibrations will result in non-dispersive (flat) lines. The comparison of the BL S_b , presented in Figure 3(a) as a color-coded map, with the graphene phonon dispersion is interesting in several respects. Despite the fact that the BL carbon atoms are not arranged in a perfect honeycomb lattice and that their IFCs present an important degree of local disorder [Figure 1(d)], S_b still displays characteristics which can be associated to a dispersive two-atom crystal. Indeed, for a fixed wavevector \mathbf{q} , the spectral function presents relative maxima at energies similar to those of graphene and, by varying \mathbf{q} , these maxima disperse, in general, in a way resembling that of graphene. The resulting brilliant stripes in Figure 3(a) display however a broadening of several meV, which is intrinsic to the BL non-crystalline nature, as well as a systematic softening *w.r.t.* graphene due to the IFCs weakening. Note, finally, that the highest optical branch near \mathbf{K} , which for graphene/graphite presents a minimum associated to a Kohn anomaly [36], becomes flat, an expected consequence of the opening of the electronic gap due to the covalent interaction with the substrate [3, 13].

The BL spectral function also determines the one-phonon Raman response. Indeed, for $\omega > 1000 \text{ cm}^{-1}$, $S_b(\omega, \mathbf{0})$ projects the BL vibrations onto the Raman active optical mode of graphene (E_{2g} , determining the G peak at $\sim 1582 \text{ cm}^{-1}$ [15]). The resulting Raman spectrum, shown in Figure 3(c), displays a minor peak at 1556 cm^{-1} (L peak) and a major band at $\sim 1475 \text{ cm}^{-1}$ (B peak). The L peak is due to vibrations localized on very short bonds and depends on the very details of the structural model. On the contrary, the B peak is a major feature of the Raman response, determined by vibra-

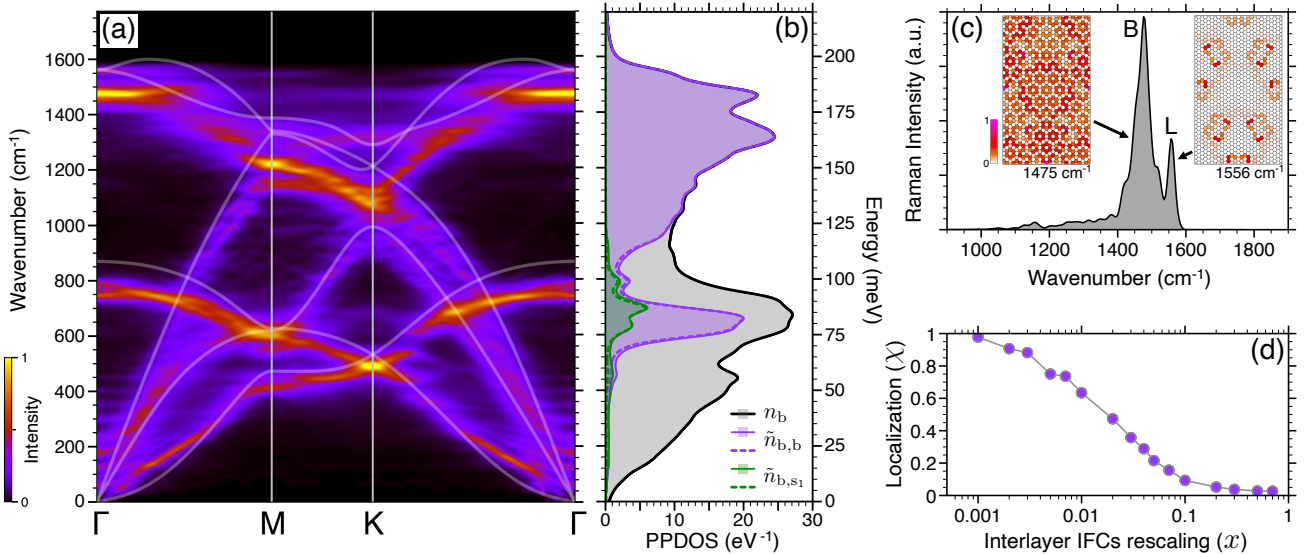


FIG. 3. (a) Calculated spectral function, $S_b(\omega, \mathbf{q})$, for heteroepitaxial BL on SiC along high-symmetry lines of the graphene Brillouin zone. White lines represent graphene phonon dispersion. (b) Buffer-layer PPDOS, n_b , from Equation 1, compared to its decomposition from Equation 2: $\tilde{n}_{b,b}$ corresponds to $l = l'$ where l is the layer index identifying the BL; for $\tilde{n}_{b,s1}$ the two indexes l and l' identify the BL and the first SiC layer. Continuous lines correspond to a slab with $L_{\text{SiC}}=30$. Dashed lines are extrapolations to a semi-infinite structure, $L_{\text{SiC}} \rightarrow \infty$. (c) Calculated BL Raman spectrum. Insets indicate the spatial distribution of the atoms contributing to the two main peaks (see SM [31]). (d) Localization of the acoustic vibrations as a function of the inter-layer IFCs (χ and x are defined in the text).

tions extending over the entire 13×13 supercell (more details in SM [31]). As a consequence, a homogeneous $(6\sqrt{3} \times 6\sqrt{3})R30^\circ$ reconstruction should present a well defined B peak whereas the presence of a broad G peak at $\sim 1582 \text{ cm}^{-1}$ should be interpreted as the signature of sample inhomogeneities. These findings help rationalize the wide range of spectral features reported for the BL. Indeed, in a first set of data [37–39], BL Raman spectra are only dominated by two broad D ($\sim 1350 \text{ cm}^{-1}$) and G ($\sim 1580\text{-}1600 \text{ cm}^{-1}$) peaks (the D peak is the typical signature of disordered carbon systems [40]). In a second set [2, 4, 41–44], the spectra are more structured and display, in addition to D and G, a usually well-defined B band at $\sim 1480\text{-}1495 \text{ cm}^{-1}$, in close agreement with our calculated frequency. According to the present results and consistently with a recent experimental analysis [20], these differences should be attributed to distinct degrees of organization in the BL structure, ranging from a disordered one in the first set of spectra to a more ordered one in the second set.

At this point, we stress that Figure 3(a) results from calculations performed on a slab containing several SiC layers, L_{SiC} . However, Figure 3(a) does not tell whether the vibrations contributing to this quasi-phonon dispersion of the BL are actually localized on the BL itself. In order to investigate this point, we need to quantify the localization of the vibrations in the direction perpendicular to the slab surface. This can be done by generalizing the

concept of inverse participation ratio [45] and defining

$$\tilde{n}_{l,l'}(\omega) = \frac{1}{N_l N_{q'}} \sum_{\nu, r, r'} |\langle l, r | e_\nu \rangle|^2 |\langle l', r' | e_\nu \rangle|^2 \delta(\omega - \omega_\nu). \quad (2)$$

When $l' = l$, the comparison of $\tilde{n}_{l,l}$ with n_l can be used to quantify how n_l , the PPDOS on layer l , is due to vibrations that are actually localized on l : within an energy region where $\tilde{n}_{l,l} \simeq n_l$, n_l is indeed due to vibrations mostly localized on layer l . On the other hand, since $n_l(\omega) = \sum_{l'} \tilde{n}_{l,l'}(\omega)$, $\tilde{n}_{l,l'}$ can be used to decompose n_l and to determine how much the modes contributing to n_l are localized on a different layer l' .

Comparing n_l and $\tilde{n}_{l,l}$ for the buffer layer [n_b and $\tilde{n}_{b,b}$ in Figure 3(b)], we first notice that below 50 meV, for $L_{\text{SiC}} \rightarrow \infty$, $\tilde{n}_{b,b} \simeq 0$ meaning that *the acoustic vibrational modes are completely delocalized on the whole SiC substrate* (see SM [31] for more details). In contrast, the vibrations corresponding to a narrow energy window centered around 80 meV, strongly relocalize on the BL, as a consequence of a gap in the phonon spectrum of SiC occurring in that energy range [31]. In the same region, a class of vibrations at $\sim 87 \text{ meV}$ display a component on the first SiC layer [$\tilde{n}_{b,s1}$ in Figure 3(b)] and can thus be interpreted as the signature of the BL/substrate covalent bonding. Note, finally, that all the vibrations above $\sim 120 \text{ meV}$ (in-plane polarized optical modes) are fully localized on the BL ($n_b \simeq \tilde{n}_{b,b}$). This obviously results from the absence of SiC vibrations in this energy range.

The complete delocalization of BL acoustic phonons

over the full SiC substrate, observed up to ~ 50 meV, has two important consequences since these vibrations determine the thermal and thermal-transport properties up to relatively high temperatures. The first one is the absence of a relevant interfacial thermal resistance between the BL and the SiC substrate (their temperatures cannot differ). The second one is that the substrate will almost entirely determine the thermal conductivity of the system. In turn, this implies that it is possible, at least in principle, to degrade thermal transport (for example by defect engineering *within* the substrate) without affecting the structure of the BL/SiC interface and, thus, the BL itself. Since the measured high charge-carrier mobility [4] is likely determined by the electronic states of the semiconducting graphitic layer, thermal transport can thus be degraded without affecting the electrical conductivity. Note that, although the thermal conductivity of hexagonal SiC is relatively high, reaching ~ 370 W/(mK) at room temperature for undoped crystals, it can be easily degraded [46].

Finally, we remark that the acoustic phonons delocalization is a very robust property of the system. Indeed, let us define a localization parameter χ for $\omega < 50$ meV vibrations as the normalized integral of $\tilde{n}_{b,b}$ (see also SM [31]). Figure 3(d) reports χ calculated for fictitious systems in which the interlayer IFCs between the BL and the substrate are rescaled by a factor x . With respect to the realistic system ($x=1$), where acoustic vibrations are delocalized on the substrate ($\chi \sim 0$), a sizable relocalization within the buffer ($\chi \sim 1$) is observed only when the interlayer IFCs are reduced to few percents of their actual *ab initio* value.

In conclusion, we performed a fully *ab initio* study of the vibrational properties of the BL/SiC system using a realistic structural model including several thousands of atoms. In spite of being a disordered form of graphene, the buffer layer still presents vibrations displaying a quasi-dispersive character resembling that of crystalline graphene. The presence of covalent bonds with the substrate results in a overall softening of the vibrations, providing a natural explanation of Raman measurements. Remarkably, as low-energy vibrations are completely delocalized on the SiC substrate, the thermal conductivity of the system is determined by the substrate itself and, thus, by its quality. This leads to an effective spatial separation between material components determining, respectively, electronic and thermal transport properties. The heteroepitaxial buffer-layer on SiC could then become a platform for thermoelectric engineering in the context of the long standing quest for a system in which the thermal conductivity can be degraded while preserving the electrical one [47].

We acknowledge support from the French Agence Nationale de la Recherche (ANR) under grants ANR-23-CE42-0028-01 (project PuMMAVi) and ANR-24-CE50-2146-02 (project BF2D). This work was granted access to the HPC resources of IDRIS under the allocations A0100910820R1 and AD010910820R2 made by Grand Equipement National de Calcul Intensif (GENCI).

The data that support the findings of this article are not publicly available. The data are available from the authors upon reasonable request.

-
- [1] C. Berger, E. H. Conrad and W. A. de Heer, *Silicon carbide and epitaxial graphene on silicon carbide in Landolt-Börnstein: Numerical Data and Functional Relationships in Science and Technology - Volume 45B, Physics of Solid Surfaces, Subvolume B*, Ed. G. Chiarotti and P. Chiaradia, Springer (2018).
- [2] M. Conrad, J. Rault, Y. Utsumi, Y. Garreau, A. Vlad, A. Coati, J.-P. Rueff, P.F. Miceli, and E.H. Conrad, Structure and evolution of semiconducting buffer graphene grown on SiC(0001), Phys. Rev. B **96**, 195304 (2017).
- [3] M.N. Nair, I. Palacio, A. Celis, A. Zobelli, A. Gloter, S. Kubsky, J.-P. Turmaud, M. Conrad, C. Berger, W. de Heer, E.H. Conrad, A. Taleb-Ibrahimi and A. Tejada, Band gap opening induced by the structural periodicity in epitaxial graphene buffer layer, Nano Lett. **17**, 2681 (2017).
- [4] J. Zhao, P. Ji, Y. Li, R. Li, K. Zhang, H. Tian, K. Yu, B. Bian, L. Hao, X. Xiao, W. Griffin, N. Dudeck, R. Moro, L. Ma and W. A. de Heer, Ultrahigh-mobility semiconducting epitaxial graphene on silicon carbide, Nature **625**, 60 (2024).
- [5] F. Iacopi and A.C. Ferrari, Tailoring graphene for electronics beyond silicon, Nature **625**, 34 (2024).
- [6] I. Forbeaux, J.M. Themlin and J.M. Debever, Heteroepitaxial graphite on 6H-SiC(0001) interface formation through conduction-band electronic structure, Phys. Rev. B **58**, 16396 (1998).
- [7] P. Mallet, F. Varchon, C. Naud, L. Magaud, C. Berger, and J.-Y. Veuillen, Electron states of mono- and bilayer graphene on SiC probed by scanning-tunneling microscopy, Phys. Rev. B **76**, 041403(R) (2007).
- [8] C. Riedl, U. Starke, J. Bernhardt, M. Franke and K. Heinz, Structural properties of the graphene-SiC(0001) interface as a key for the preparation of homogeneous large-terrace graphene surfaces, Phys. Rev. B **76**, 245406 (2007).
- [9] K.V. Emtsev, F. Speck, T. Seyller, L. Ley and J.D. Riley, Interaction, growth, and ordering of epitaxial graphene on SiC{0001} surfaces: A comparative photoelectron spectroscopy study, Phys. Rev. B **77**, 155303 (2008).
- [10] S. Kim, J. Ihm, H.J. Choi and Y.-W. Son, Origin of Anomalous Electronic Structures of Epitaxial Graphene on Silicon Carbide, Phys. Rev. Lett. **100**, 176802 (2008).
- [11] F. Varchon, P. Mallet, J.-Y. Veuillen and L. Magaud, Ripples in epitaxial graphene on the Si-terminated SiC(0001) surface, Phys. Rev. B **77**, 235412 (2008).
- [12] I. Deretzis and A. La Magna, Role of covalent and metallic intercalation on the electronic properties of epitaxial

- graphene on SiC(0001), Phys. Rev. B **84**, 235426 (2011).
- [13] T. Cavallucci and V. Tozzini, Intrinsic structural and electronic properties of the Buffer Layer on Silicon Carbide unraveled by Density Functional Theory, Sci. Rep. **8**, 13097 (2018).
- [14] A.C. Ferrari, J.C. Meyer, V. Scardaci, C. Casiraghi, M. Lazzeri, F. Mauri, S. Piscanec, D. Jiang, K.S. Novoselov, S. Roth, and A.K. Geim, Raman Spectrum of Graphene and Graphene Layers, Phys. Rev. Lett. **97**, 187401 (2006).
- [15] A.C. Ferrari and D.M. Basko, Raman spectroscopy as a versatile tool for studying the properties of graphene, Nature Nanotech. **8**, 235 (2013).
- [16] A. Armano and S. Agnello, Two-Dimensional Carbon: A Review of Synthesis Methods, and Electronic, Optical, and Vibrational Properties of Single-Layer Graphene, C. **5**, 67 (2019).
- [17] Y. Anno, Y. Imakita, K. Takei, S. Akita and T. Arie, Enhancement of graphene thermoelectric performance through defect engineering, 2D Mater. **4**, 025019 (2017).
- [18] P. Zong, J. Liang, P. Zhang, C. Wan, Y. Wang, and K. Koumoto, Graphene-Based Thermoelectrics, ACS Appl. Energy Mater. **3**, 2224 (2020).
- [19] V. Rathi, R. Brajpuria, R. Gupta, K.P.S. Parmar and A. Kumar, Graphene-derived composites: a new frontier in thermoelectric energy conversion, Energy Adv. **3**, 389 (2024).
- [20] T. Wang, J.-R. Huntzinger, M. Bayle, C. Roblin, J.-M. Decams, A.-A. Zahab, S. Contreras, M. Paillet and P. Landois, Buffer layers inhomogeneity and coupling with epitaxial graphene unravelled by Raman scattering and graphene peeling, Carbon **163**, 224 (2020).
- [21] F. Fromm, M.H. Oliveira Jr, A. Molina-Sánchez, M. Hundhausen, J.M.J. Lopes, H. Riechert, L. Wirtz, and T. Seyller, Contribution of the buffer layer to the Raman spectrum of epitaxial graphene on SiC(0001), New J. of Phys. **15**, 043031 (2013).
- [22] E. Minamitani, R. Arafune, T. Frederiksen, T. Suzuki, S. Mohammad Fakruddin Shahed, T. Kobayashi, N. Endo, H. Fukidome, S. Watanabe and T. Komeda, Atomic-scale characterization of the interfacial phonon in graphene/SiC, Phys. Rev. B **96**, 155431 (2017).
- [23] T. Milenov, P. Rafailov, R. Yakimova, I. Shtepliuk and V. Popov, Raman fingerprint of the graphene buffer layer grown on the Si-terminated face of 4H-SiC(0001): Experiment and theory, J. Raman Spectrosc. **55**, 416 (2024).
- [24] S. Baroni, S. de Gironcoli, A. Dal Corso and P. Giannozzi, Phonons and related crystal properties from density-functional perturbation theory, Rev. Mod. Phys. **73**, 515 (2001).
- [25] P. Giannozzi, S. Baroni, N. Bonini, M. Calandra, R. Car, C. Cavazzoni, D. Ceresoli, G.L. Chiarotti, M. Cococcioni, I. Dabo *et al.*, QUANTUM ESPRESSO: a modular and open-source software project for quantum simulations of materials, J. Phys.: Condens. Matt. **21**, 395502 (2009).
- [26] M. Schlipf and F. Gygi, Optimization algorithm for the generation of ONCV pseudopotentials, Computer Phys. Comm. **196**, 36 (2015).
- [27] J.P. Perdew, K. Burke and M. Ernzerhof, Generalized gradient approximation made simple, Phys. Rev. Lett. **77**, 3865 (1996).
- [28] F.S. Hage, G. Radtke, D.M. Kepaptsoglou, M. Lazzeri and Q.M. Ramasse, Single-atom vibrational spectroscopy in the scanning transmission electron microscope, Science **367**, 1124 (2020).
- [29] C. Bungaro, S. de Gironcoli and S. Baroni, Theory of the anomalous Rayleigh dispersion at H/W(110) surfaces, Phys. Rev. Lett. **77**, 2491 (1996).
- [30] M. Lazzeri and P. Thibaudeau, *Ab initio* Raman spectrum of the normal and disordered MgAl₂O₄ spinel, Phys. Rev. B **74**, 140301 (2006).
- [31] See Supplemental Material at XXX for additional information on the density functional theory calculations for bulk 4H-SiC and $(6\sqrt{3} \times 6\sqrt{3})R30^\circ$ surface reconstruction, a more precise mathematical definition of the reported quantities, details on the Raman spectrum modeling and on the procedure devised to extrapolate the results to the limit of a semi-infinite substrate.
- [32] F.H. Allen, O.Kennard, D.G. Watson, L. Brammer, A.G. Orpen and R. Taylor, Tables of bond lengths determined by X-ray and neutron diffraction. Part 1. Bond lengths in organic compounds, J. Chem. Soc., Perkin Trans. 2 **S1** (1987).
- [33] W. Chen, H. Xu, L. Liu, X. Gao, D. Qi, G. Peng, S. Ching Tan, Y. Feng, K.P. Loh and A.T.S. Wee, Atomic structure of the 6H-SiC(0001) nanomesh, Surf. Sci. **596**, 176 (2005).
- [34] I. Palacio, A. Celis, M.N. Nair, A. Gloter, A. Zobelli, M. Sicot, D. Malterre, M.S. Nevius, W.A. de Heer, C. Berger E.H. Conrad, A. Taleb-Ibrahimi and A. Tejada, Atomic structure of epitaxial graphene sidewall nanoribbons: flat graphene, miniribbons, and the confinement gap, Nano Lett. **15**, (2015).
- [35] J. Hass, J.E. Millán-Otoya, P.N. First and E. H. Conrad, Interface structure of epitaxial graphene grown on 4H-SiC(0001), Phys. Rev. B **78**, 205424 (2008).
- [36] S. Piscanec, M. Lazzeri, F. Mauri, A.C. Ferrari and J. Robertson, Kohn anomalies and electron-phonon interactions in graphite, Phys. Rev. Lett. **93**, 185503 (2004).
- [37] T. Schumann, M. Dubsclaff, M.H. Oliveira, Jr., M. Hanke, J.M.J. Lopes and H. Riechert, Effect of buffer layer coupling on the lattice parameter of epitaxial graphene on SiC(0001), Phys. Rev. B **90**, 041403(R) (2014).
- [38] W. Strupinski, K. Grodecki, P. Caban, P. Ciepielewski, I. Jozwik-Biala, J.M. Baranowski, Formation mechanism of graphene buffer layer on SiC(0001), Carbon **81**, 63 (2015).
- [39] M. Kruskopf, K. Pierz, D. Momeni Pakdehi, S. Wundrack, R. Stosch, A. Bakin, H.W. Schumacher, A morphology study on the epitaxial growth of graphene and its buffer layer, Thin Solid Films **659**, 7 (2018).
- [40] A.C. Ferrari and J. Robertson, Interpretation of Raman spectra of disordered and amorphous carbon, Phys. Rev. B **61**, 14095 (2000).
- [41] J. Bao, W. Norimatsu, H. Iwata, K. Matsuda, T. Ito and M. Kusunoki, Synthesis of freestanding graphene on SiC by a rapid-cooling technique, Phys. Rev. Lett. **117**, 205501 (2016).
- [42] M. Kruskopf, D.M. Pakdehi, K. Pierz, S. Wundrack, R. Stosch, T. Dziomba, M. Götz, J. Baringhaus, J. Aprozanz, C. Tegenkamp, J. Lidzba, T. Seyller, F. Hohls, F. J Ahlers and H.W. Schumacher, Comeback of epitaxial graphene for electronics: large-area growth of bilayer-free graphene on SiC, 2D Mater. **3**, 041002 (2016).
- [43] S. Wundrack, D. Momeni Pakdehi, P. Schädlich, F. Speck, K. Pierz, T. Seyller, H.W. Schumacher, A. Bakin and R. Stosch, Probing the structural transition from buffer layer to quasifreestanding monolayer graphene by

- Raman spectroscopy, *Phys. Rev. B* **99**, 045443 (2019).
- [44] M. Rejhon and J. Kunc, ZO phonon of a buffer layer and Raman mapping of hydrogenated buffer on SiC(0001), *J. Raman Spectrosc.* **50**, 465 (2018).
- [45] F. Wegner, Inverse participation ratio in $2+\epsilon$ dimensions, *Zeitsch. Phys. B Condens. Matt.* **3**, 209 (1980).
- [46] G.A. Slack, Thermal conductivity of pure and impure silicon, silicon carbide, and diamond, *J. App. Phys.* **35**, 3460 (1964).
- [47] G.J. Snyder and E.S. Toberer, Complex thermoelectric materials, *Nature Mater.* **7**, 105 (2008).